ACS Photonics

pubs.acs.org/journal/apchd5

Article

Computational Nonscanning Incoherent Superoscillatory Imaging

Haitang Yang,* Esther Y. H. Lin, Kiriakos N. Kutulakos, and George V. Eleftheriades

Cite This: *ACS Photonics* 2022, 9, 290–295

Read Online

ACCESS | Metrics & More | Article Recommendations | Supporting Information

ABSTRACT: Superoscillatory (SO) imaging is an emerging technique to super-resolve unlabeled objects in the far-field. Reducing the full width at half-maximum (FWHM) of the main beam is a standard method used in SO imaging to pursue a finer resolution. However, reducing the FWHM dims the main beam sharply. This results in very poor signal-to-noise ratios that are beyond the capability of conventional image sensors. We present an approach that does not seek to reduce the FWHM of the main beam. Instead, we describe an imaging system whose SO point spread function is very broad, yet preserves sufficiently high frequencies to enable sharp image reconstruction by computational deconvolution. A key observation in this work is that deconvolution-based SO imaging is only possible for SO systems that are incoherent; we show how to realize such a system with a red light-emitting diode and a programmable spatial light modulator. This system enables the application of standard deconvolution algorithms to image subdiffraction objects in a single shot without any form of scanning. Overall, we demonstrate computational SO imaging of previously unseen 2D complex objects with a submicron resolution that is one-fifth the diffraction limit.

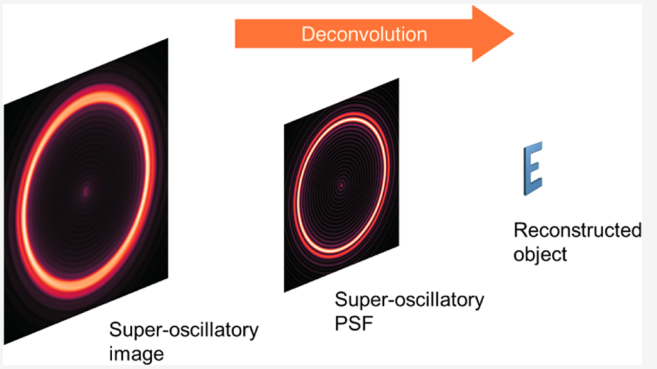

KEYWORDS: *computational imaging, nonscanning imaging, incoherent imaging, superoscillatory imaging, submicron resolution, super-resolution imaging*

1. INTRODUCTION

All optical imaging systems suffer from one fundamental constraint in resolution—the diffraction limit. Currently, the field of super-resolution imaging aims to overcome this resolution barrier with various techniques such as stimulated-emission-depletion fluorescence microscopy,[1] photoactivated localization microscopy[2] and stochastic optical reconstruction microscopy,[3] all of which rely on prior fluorescence labeling. Superoscillation is a phenomenon where parts of a signal oscillate faster than their highest Fourier component.[4−6] This characteristic frees superoscillatory (SO) imaging from labeling-associated constraints and enables imaging beyond the diffraction limit in far-field regimes.[7−9]

While advancements have been made in the field of SO imaging,[10,11] there remain challenges that hinder its development and practicality. One major issue is the low signal-to-noise ratio (SNR) in the region of interest (ROI) attributed to the high dynamic range spanned by weak superoscillations and strong sidebands (see Figure 1a,b) in SO point spread functions (PSFs). In addition, reducing the full width at half maximum (FWHM) of the SO PSF's main beam, a technique commonly used in current SO imaging for pursuing finer resolutions, exacerbates this issue. The tradeoff to producing faster superoscillations with a narrower main beam is an exponential increase in the sideband intensity, as shown in Figure 1c. Increasing the sideband intensity therefore reduces sharply the illumination energy used to form the super-resolved image in the ROI, which is already a minute fraction of the energy deposited in the sidebands. This results in extremely low SNRs. Although high dynamic range imaging[12] can improve image quality to some extent despite the low SNR, this requires very long exposure times and potentially multiple image captures, making it unsuitable for imaging dynamic phenomena.

Our approach is based on the observation that there is considerable high-frequency detail in the sidebands of SO PSFs. To exploit it, we use the full SO PSF—including the sidebands—and process the acquired SO image computationally via deconvolution. This removes our system's dependence on the main beam's FWHM and allows us to utilize SO PSFs that yield a far higher SO image SNR than previous methods.

Previous work on SO imaging was centered on designing SO PSFs whose main beam exhibits faster oscillations than those found in the diffraction-limited PSF. With these engineered SO PSFs, SO imaging systems are operated as conventional coherent optical microscopes. These coherent systems domi-

Received: October 30, 2021
Published: December 14, 2021

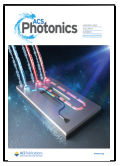

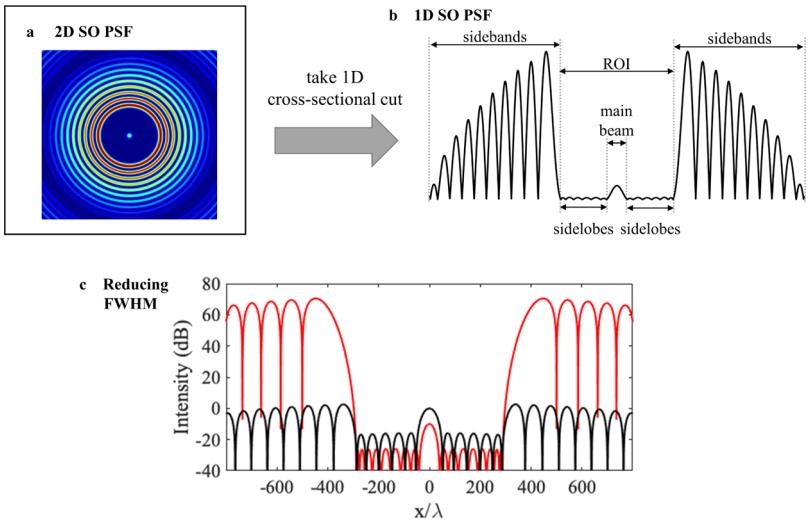

Figure 1. (a,b) Main components of an SO PSF. (c) Reducing the FWHM of an SO PSF (black line) increases the sideband intensity (red line) exponentially.

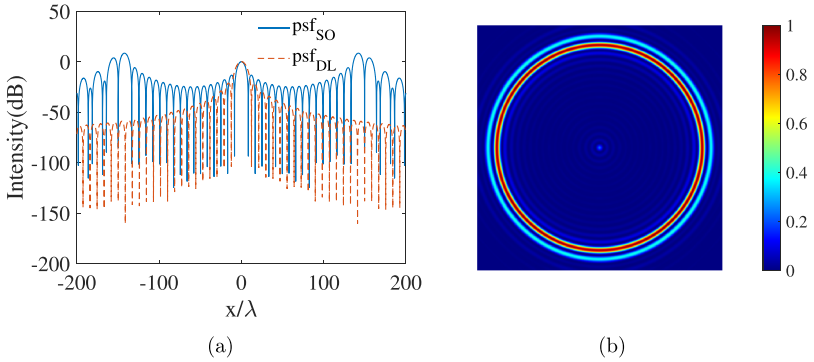

Figure 2. (a) 1D and (b) 2D SO PSF. psf_{SO} and psf_{DL} denote the SO and diffraction-limited system PSF, respectively.

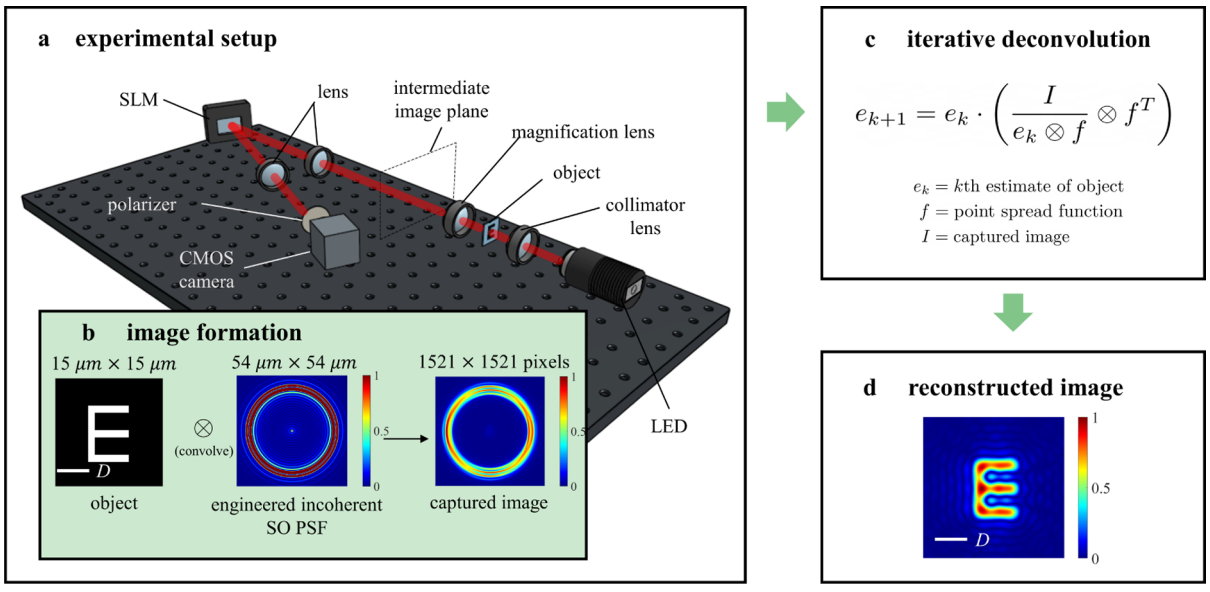

Figure 3. Computational SO imaging model including the (a) incoherent SO imaging system with a magnification equal to 15×, (b) simulated image formation process in our system (the scale bar D denotes the diffraction limit), (c) deconvolution algorithm applied to the captured image via the engineered PSF, and (d) reconstructed image. We use a narrow-band 625 nm LED M625L4 to enforce spatial incoherence. Our SLM modulates the red light polarized along the long display axis. A polarizer is used to filter out the components polarized perpendicular to the long display axis.

nate current SO imaging, with specific techniques involving SO light illumination,[13−16] modulated optical transfer functions,[9,17,18] and aperture engineering.[19,20] Building a coherent SO imaging system, however, requires careful navigation of a

https://doi.org/10.1021/acsphotonics.1c01672
ACS Photonics 2022, 9, 290−295

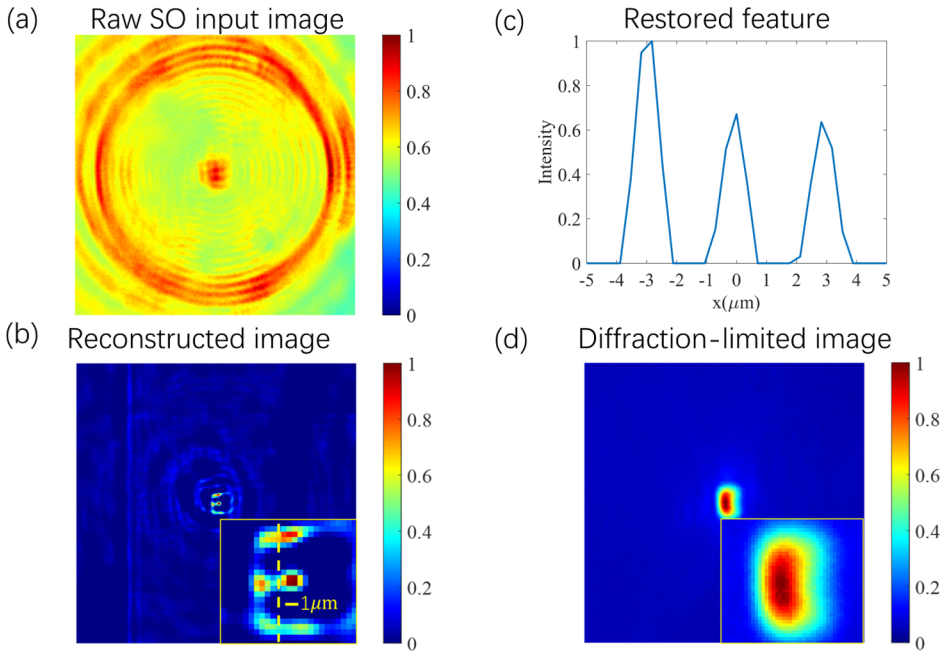

Figure 4. Reconstruction of the object of letter ***E***, where (a) is the raw input SO image into the deconvolution algorithm, (b) is the output of the deconvolution algorithm with a zoomed-in view of the restored object provided in the inset, (c) is a cross section of the restored object marked by the yellow dashed line in the inset of (b), and (d) is the diffraction-limited image for comparison. The features in (c) are used to determine the resolution.

critical tradeoff in the SO PSF design: while it is possible to create PSFs with rapid fluctuations well beyond the diffraction limit within a spatially compact region (called the "main beam"), doing so subsequently produces fluctuations of lower frequency and significantly higher intensity outside it. To date, past work has focused exclusively on one particular way to take advantage of this tradeoff: make the main beam as narrow as possible while simultaneously maximizing the separation between the main beam and the PSF's low-frequency regions (i.e., the sidebands). Unfortunately, this strategy leads to extremely low SNRs, as explained earlier.

To achieve high-SNR SO imaging, we explore the spatially incoherent system shown in Figure 3a. The system's spatial incoherence enforces a convolutional model for SO image formation, enabling use of conventional deconvolution techniques to restore images of general, previously unseen objects at a resolution far beyond the diffraction limit. In this model, the captured image is the convolution of an intensity image with an intensity SO PSF. This model, which is not valid for coherent SO imaging, relaxes our PSF design considerations to a single requirement: ensure that enough high-frequency-preserving fluctuations exist somewhere in the PSF—be it sidelobes, sidebands, and/or main beam—so that the object's image can be restored via deconvolution.

While incoherent illumination sources have been used for SO imaging previously, they were utilized for a different purpose, namely, broadband super-resolution imaging[21] or imaging an in-phase two-aperture object.[22] Crucially, these methods rely on the main beam's FWHM for imaging, and thus they suffer from the same SNR limitations discussed previously. Our work, on the other hand, uses incoherence as a means to achieve high-SNR SO imaging via deconvolution and via engineered PSFs whose high frequencies occur well beyond the main beam. We show that this enables imaging of complex objects with a resolution much finer than what the FWHM of the main beam would allow. In this respect, an important contribution of our work is to show that SO imaging and computational techniques can be combined to push the state of the art in subdiffraction imaging of general objects.

Last, the method proposed by Pu et al.[23,24] constructs a deep network to infer the dimensions and locations of various dimers with subdiffraction spacings. While their approach shows that SO imaging and neural networks can be combined to localize and identify objects in an SO image, given sufficient training data, this approach essentially relies on object classification and hence is unsuitable for subdiffraction imaging of objects that were not seen during training. Moreover, their system has a very narrow field of view that necessitates scanning, which is time-consuming and requires precise mechanical positioning. Since our approach relies on image deconvolution and does not require a training set, it imposes no constraints on the objects being imaged, and its performance is not dependent on whether or not the object is known or seen before. In addition, our system needs no scanning and requires capturing only a single image of the object.

To summarize, our computational approach offers four contributions to SO-based super-resolution imaging. First and foremost, we demonstrate single-shot imaging of previously unseen 2D objects at one-fifth the diffraction limit via superoscillation. Second, incorporating incoherence and computational deconvolution into SO imaging, we show that it is possible to relax SO PSF design constraints. This allows us to boost the image SNR significantly compared to past work. Third, our method is only concerned with preserving and restoring high-frequency features in the SO PSF without imposing restrictions on their location within it. We thus use the full SO PSF for imaging, which makes our system much more resilient to noise. Fourth, our deconvolution image formation model is fully general and does not assume any knowledge of the 2D object being imaged.

https://doi.org/10.1021/acsphotonics.1c01672
ACS Photonics 2022, 9, 290−295

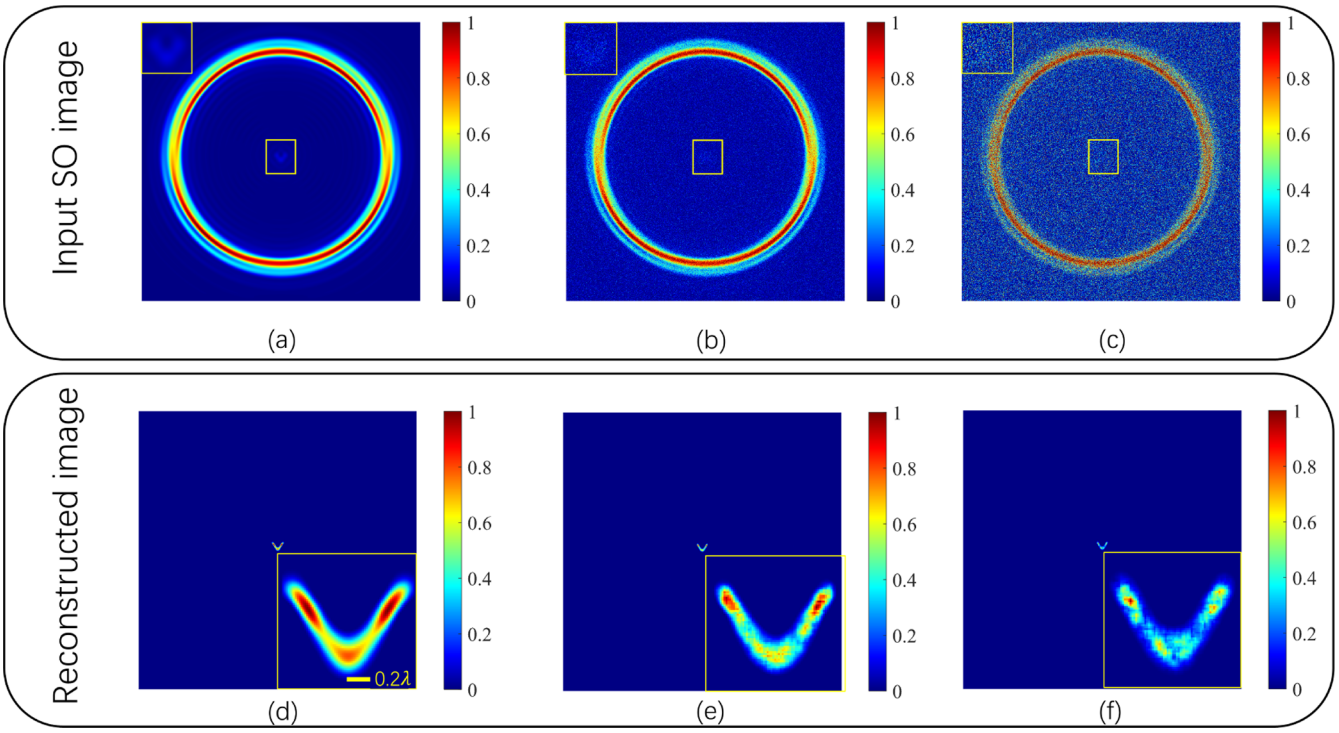

Figure 5. Deconvolution of simulated SO images corrupted by noise. In the top row, we have SO images that are corrupted with different levels of noise. These noise-corrupted images are input into the deconvolution algorithm. In the bottom row, we have the output of the deconvolution algorithm containing the restored objects. The SO image (a) is corrupted with Poisson noise, (b) with Gaussian noise $\sim N(0,10^{-2})$, and (c) with Gaussian noise $\sim N(0,10^{-1})$. Deconvolution results (d) correspond to (a), (e) to (b), and (f) to (c). The insets on the top-left corner are the enlarged versions of the corrupted super-resolved images within the yellow-lined rectangles. The insets on the bottom-right corner are the enlarged versions of the restored images.

2. METHOD

2.1. Limitations of Conventional SO Imaging. Conventional SO imaging prefers the technique of decreasing the main beamwidth for improving super-resolution. However, decreasing the main beamwidth results in the rise of sideband intensity. As a result, the super-resolved image in the ROI will weaken, rendering SO imaging more susceptible to noise corruption while also growing in the dynamic range, going beyond the camera capabilities. To circumvent these difficulties, we propose our computational nonscanning incoherent SO imaging (CNISI) model.

2.2. CNISI Model. In the conventional SO imaging model, the main beam is expected to have a narrower FWHM, which reduces the SNR in the ROI by raising the sidebands. In the computational incoherent SO imaging model (see Figure 3), however, it is not necessary to pursue a highly shrunken main beam. Instead, the object is reconstructed subsequently by applying deconvolution algorithms to the incoherent SO image.

Experiments are conducted in an incoherent imaging system composed of a one-lens magnification imaging system and a cascaded two-lens 4F imaging system, as shown in Figure 3a. By prepending a magnification imaging system, we can make the intermediate image plane the object plane of the subsequent 4F system. Within the 4F system, a programmable spatial light modulator (SLM) placed on the Fourier plane modulates the coefficients of the frequency components of the object. This SLM (LETO phase-only SLM) has 1920 × 1080 pixels with a pitch of 6.4 μm and has an active area of 12.5 × 7.1 mm2. After reflection from the SLM, light is focused by an imaging lens onto a CMOS camera.

The SO imaging can be presented by

$$\text{imag} = \text{obj} \otimes \text{psf} \tag{1}$$

where obj is the intensity object, $\otimes$ denotes the convolution, and psf is the incoherent system PSF, given by (see Section S6 in the Supporting Information for the complete derivation)

$$\text{psf} = |\text{psf}_1 \otimes \text{psf}_2|^2 \tag{2}$$

where psf_1 is the PSF of the magnification system and psf_2 is the PSF of the cascaded 4F system. In our incoherent imaging system, psf_1 is a magnified diffraction-limited PSF and psf_2 is engineered to be an SO PSF (see Section S1 in the Supporting Information for the engineering method and characteristics of our SO PSF). The SO system PSF for our experiments is shown in Figure 2. Equipped with the incoherent SO PSF, we are ready to conduct incoherent SO imaging and perform deconvolution on SO images for object reconstructions.

3. EXPERIMENTAL RESULTS

The SO image for the letter ***E*** etched on a chromium film (see Figure S4 in the Supporting Information for detailed information) captured within our incoherent SO imaging system is shown in Figure 4a. Experimental SO images and the simulated theoretical SO PSF are provided as input to the Richardson–Lucy deconvolution algorithm.[25,26] The outputs of the deconvolution algorithm are the object reconstructions. This deconvolution algorithm is given by[27]

$$e_{k+1} = e_k \cdot \left(\frac{I}{e_k \otimes f} \otimes f^{\mathrm{T}} \right) \tag{3}$$

https://doi.org/10.1021/acsphotonics.1c01672
ACS Photonics 2022, 9, 290−295

where e_k is the kth estimate of the object, I is the input image that is also equal to e_0, f is the PSF, and f^T is the transpose of f. The Richardson−Lucy algorithm has been widely applied to the field of microscopy, such as confocal microscopy,[28,29] structured illumination microscopy,[30,31] and so forth.[32]

The successfully reconstructed letter ***E*** is displayed in Figure 4b and is of much higher resolution compared to the diffraction-limited image in Figure 4d. To estimate the restored resolution, we measure the widths of the three strokes of the restored letter ***E***, as shown in Figure 4c. The measured feature FWHMs of the three strokes are 0.9180 μm, 0.9187 μm, and 0.9190 μm, the average of which is 0.92 μm (with two significant figures). This restored resolution is one-fifth the diffraction limit (see Section S2 in the Supporting Information for the measured diffraction limit). Our computational SO imaging demonstrates significant improvement in resolution compared to the imaging results of 2D complex objects in refs 17 and 21. Section S3 in the Supporting Information explains how this restored resolution is obtained. Our reconstruction results on the additional object of letter ***V*** are provided in Section S4 of the Supporting Information. While the supplementary also elaborates on the differences between our method and conventional SO imaging, one significant difference in the context of resolution is that the deconvolution applied to images captured with our system is independent of the super-resolution image within the ROI, whereas conventional SO imaging is not.

4. DISCUSSION

4.1. Noise Analysis. An extended noise analysis is provided in Section S5 of the Supporting Information. According to our analysis, there are two dominant sources of noise in our system. The first is the noise described by the Poisson distribution, including dark current and photon noise that increases with the intensity of the image.[33] The second follows a Gaussian distribution, including the read noise from the sensor readout and the ADC noise generated by the analog-to-digital converter.[12] The contributions from these two types of noise are included in our simulations, where we investigate the effect of noise on object restoration. The simulation results are depicted in Figure 5, showing that deconvolution results are resilient against the addition of noise. Although the SNR is −0.3 dB in Figure 5c, the profile of the object can still be reconstructed.

4.2. Comparison. A PSF feature extraction algorithm is proposed with only simulation results to recover the object of two apertures from an incoherent SO image in ref 34. This algorithm uses

$$\text{img} = \text{psf}_{\text{SO}} \otimes \text{obj} \tag{4}$$

where

$$\text{obj} = \sum_n \delta(x - x_n, y - y_n) \tag{5}$$

Thus

$$\text{img} = \sum_n \text{psf}_{\text{SO}}(x - x_n, y - y_n) \tag{6}$$

Based on the decomposition of the image, every Dirac delta function $\delta(x - x_n, y - y_n)$ can be located by a matching pattern with a specific intensity threshold. This matching pattern is composed of two concentric circles, whose radii and thresholds are in accordance with the two sidebands with the highest intensity. The recovered resolution is only 0.67 times the diffraction limit. Furthermore, the noise may weaken the applicability of this algorithm in terms of the necessary precise intensity threshold. This algorithm needs to scan the entire SO image, whereas an iterative nonscanning algorithm is used in this paper.

4.3. Perspective on Resolution Improvement. In this paper, our diffraction limit is 4.9 μm, which is equivalent to numerical aperture (NA) = 0.08. By replacing the lens in our one-lens magnification system with an objective lens of NA = 1 or with a commercial nonscanning conventional microscope, the resolution can be theoretically improved to 200/5 = 40 nm. This resolution is comparative to typical optical nanoscopies enabled by our far-field, nonfluorescence, and nonscanning scheme. During the acquisition of our measurements, we found that alignment significantly affects the resolution and the ring structures of the SO image. This is challenging because the deconvolution process relies considerably on the ring structures. When using a high-NA objective lens, the optical aberrations also deteriorate the ring structures. Thus, precise alignment and aberration corrections are essential for reducing variability in our deconvolution results and upgrading our CNISI system.

5. CONCLUSIONS

While reducing the FWHM is a popular technique for resolution improvement in conventional SO microscopy, the resultant intensity increase in sidebands would lower the SNR in the ROI. Therefore, to further improve the resolution without any decline in the SNR, we approach SO imaging from a different perspective. We impose a convolutional image formation model where the object restoration (deconvolution result) is independent of the super-resolution image in the ROI. Our experimental implementation consists of a cascaded imaging system composed of a one-lens microscope (easily replaceable for resolution improvement) and a 4F system with a programmable SLM placed on the Fourier plane. SO masks are displayed on the SLM, modulating the diffraction-limited Airy disk PSF into an SO PSF. We then utilize the Richardson−Lucy deconvolution algorithm on captured images to reconstruct complex 2D objects from the experimental SO images. Our results achieve a submicron-reconstructed resolution one-fifth the diffraction limit. To pursue a higher resolution, the only modification needed is replacing the current one-lens microscope with a higher-NA microscope.

This work demonstrates that incoherence can be combined with SO imaging to reconstruct objects with finer resolutions than the designed SO PSF. Furthermore, our method is robust to noise and generalized for 2D objects. Overall, we present a new technique that integrates computational methods with SO imaging while also relaxing the current limitations on the SO PSF design.

■ ASSOCIATED CONTENT

Supporting Information

The Supporting Information is available free of charge at https://pubs.acs.org/doi/10.1021/acsphotonics.1c01672.

Additional simulations and measurement data (PDF)

■ AUTHOR INFORMATION

Corresponding Author

Haitang Yang − *The Edward S. Rogers Sr. Department of Electrical and Computer Engineering, University of Toronto,*

https://doi.org/10.1021/acsphotonics.1c01672
ACS Photonics 2022, 9, 290−295

Toronto, Ontario M5S 3G4, Canada; orcid.org/0000-0001-8833-1071; Email: haitang.yang@mail.utoronto.ca

Authors

Esther Y. H. Lin − *Department of Computer Science, University of Toronto, Toronto, Ontario M5S 3G4, Canada*

Kiriakos N. Kutulakos − *Department of Computer Science, University of Toronto, Toronto, Ontario M5S 3G4, Canada*

George V. Eleftheriades − *The Edward S. Rogers Sr. Department of Electrical and Computer Engineering, University of Toronto, Toronto, Ontario M5S 3G4, Canada;* orcid.org/0000-0001-7987-3864

Complete contact information is available at: https://pubs.acs.org/10.1021/acsphotonics.1c01672

Funding

This research is funded by the Government of Canada Tri-agency New Frontiers in Research Fund (NFRF).

Notes

The authors declare no competing financial interest.

REFERENCES

(1) Hell, S. W.; Wichmann, J. Breaking the diffraction resolution limit by stimulated emission: stimulated-emission-depletion fluorescence microscopy. *Opt. Lett.* **1994**, *19*, 780−782.

(2) Betzig, E.; Patterson, G. H.; Sougrat, R.; Lindwasser, O. W.; Olenych, S.; Bonifacino, J. S.; Davidson, M. W.; Lippincott-Schwartz, J.; Hess, H. F. Imaging intracellular fluorescent proteins at nanometer resolution. *Science* **2006**, *313*, 1642−1645.

(3) Rust, M. J.; Bates, M.; Zhuang, X. Sub-diffraction-limit imaging by stochastic optical reconstruction microscopy (STORM). *Nat. Methods* **2006**, *3*, 793−796.

(4) Berry, M. V. Faster than Fourier. In *Quantum Coherence and Reality; in Celebration of the 60th Birthday of Yakir Aharonov*; Anandan, J. S., Safko, J. L., Eds.; World Scientific, 1994; pp 55−65.

(5) Ferreira, P. J. S. G.; Kempf, A. Superoscillations: faster than the Nyquist rate. *IEEE Trans. Signal Process.* **2006**, *54*, 3732−3740.

(6) Zheludev, N. I. What diffraction limit? *Nat. Mater.* **2008**, *7*, 420−422.

(7) Berry, M. V.; Popescu, S. Evolution of quantum superoscillations and optical superresolution without evanescent waves. *J. Phys. A: Math. Gen.* **2006**, *39*, 6965.

(8) Rogers, E. T. F.; Lindberg, J.; Roy, T.; Savo, S.; Chad, J. E.; Dennis, M. R.; Zheludev, N. I. A super-oscillatory lens optical microscope for subwavelength imaging. *Nat. Mater.* **2012**, *11*, 432−435.

(9) Wong, A. M.; Eleftheriades, G. V. An optical super-microscope for far-field, real-time imaging beyond the diffraction limit. *Sci. Rep.* **2013**, *3*, 1715.

(10) Chen, G.; Wen, Z.-Q.; Qiu, C.-W. Superoscillation: from physics to optical applications. *Light Sci. Appl.* **2019**, *8*, 56.

(11) Berry, M.; Zheludev, N.; Aharonov, Y.; Colombo, F.; Sabadini, I.; Struppa, D. C.; Tollaksen, J.; Rogers, E. T.; Qin, F.; Hong, M.; et al. Roadmap on superoscillations. *J. Opt.* **2019**, *21*, 053002.

(12) Hasinoff, S. W.; Durand, F.; Freeman, W. T. Noise-optimal capture for high dynamic range photography. *Proceedings 23rd IEEE Conference on Computer Vision and Pattern Recognition*, 2010; pp 553−560.

(13) Rogers, E. T. F.; Quraishe, S.; Rogers, K. S.; Newman, T. A.; Smith, P. J. S.; Zheludev, N. I. Far-field unlabeled super-resolution imaging with superoscillatory illumination. *APL Photonics* **2020**, *5*, 066107.

(14) Yuan, G. H.; Lin, Y.-H.; Tsai, D. P.; Zheludev, N. I. Superoscillatory quartz lens with effective numerical aperture greater than one. *Appl. Phys. Lett.* **2020**, *117*, 021106.

(15) Deng, Z.; Shapira, N.; Remez, R.; Li, Y.; Arie, A. Talbot effect in waveforms containing subwavelength multilobe superoscillations. *Opt. Lett.* **2020**, *45*, 2538−2541.

(16) Shapira, N.; Deng, Z.; Remez, R.; Singh, D.; Katzav, E.; Arie, A. Multi-lobe superoscillation and its application to structured illumination microscopy. *Opt. Express* **2019**, *27*, 34530−34541.

(17) Dong, X. H.; Wong, A. M. H.; Kim, M.; Eleftheriades, G. V. Superresolution far-field imaging of complex objects using reduced superoscillating ripples. *Optica* **2017**, *4*, 1126−1133.

(18) Yang, H.; Eleftheriades, G. V. Synthesis of Super-Oscillatory Point-Spread Functions with Taylor-Like Tapered Sidelobes for Advanced Optical Super-Resolution Imaging. *Photonics* **2021**, *8*, 64.

(19) Smith, M. K.; Gbur, G. Mathematical method for designing superresolution lenses using superoscillations. *Opt. Lett.* **2020**, *45*, 1854−1857.

(20) Xie, Q.; Jiang, Y.; Liang, J.; Qu, E.; Ren, L. Hybrid phase-amplitude superoscillation element for nonscanning optical super-resolution imaging. *J. Opt. Soc. Am. A* **2019**, *36*, 196−201.

(21) Li, Z.; Zhang, T.; Wang, Y.; Kong, W.; Zhang, J.; Huang, Y.; Wang, C.; Li, X.; Pu, M.; Luo, X. Achromatic Broadband super-resolution imaging by super-oscillatory metasurface. *Laser Photon. Rev.* **2018**, *12*, 1800064.

(22) Xie, Q.; Jiang, Y.; Liang, J.; Qu, E.; Ren, L. Incoherent, non-invasive and non-scanning superoscillation-based microscope for super-resolution imaging. *Opt. Commun.* **2020**, *463*, 125445.

(23) Pu, T.; Ou, J. Y.; Savinov, V.; Yuan, G.; Papasimakis, N.; Zheludev, N. I. Unlabeled Far-Field Deeply Subwavelength Topological Microscopy (DSTM). *Adv. Sci.* **2021**, *8*, 2002886.

(24) Pu, T.; Ou, J. Y.; Papasimakis, N.; Zheludev, N. I. Label-free deeply subwavelength optical microscopy. *Appl. Phys. Lett.* **2020**, *116*, 131105.

(25) Richardson, W. H. Bayesian-based iterative method of image restoration. *J. Opt. Soc. Am.* **1972**, *62*, 55−59.

(26) Lucy, L. B. An iterative technique for the rectification of observed distributions. *Astron. J.* **1974**, *79*, 745.

(27) Guo, M.; Li, Y.; Su, Y.; Lambert, T.; Nogare, D. D.; Moyle, M. W.; Duncan, L. H.; Ikegami, R.; Santella, A.; Rey-Suarez, I.; et al. Rapid image deconvolution and multiview fusion for optical microscopy. *Nat. Biotechnol.* **2020**, *38*, 1337−1346.

(28) Laasmaa, M.; Vendelin, M.; Peterson, P. Application of regularized Richardson−Lucy algorithm for deconvolution of confocal microscopy images. *J. Microsc.* **2011**, *243*, 124−140.

(29) Dey, N.; Blanc-Feraud, L.; Zimmer, C.; Roux, P.; Kam, Z.; Olivo-Marin, J.-C.; Zerubia, J. Richardson−Lucy algorithm with total variation regularization for 3D confocal microscope deconvolution. *Microsc. Res. Tech.* **2006**, *69*, 260−266.

(30) Ströhl, F.; Kaminski, C. F. A joint Richardson—Lucy deconvolution algorithm for the reconstruction of multifocal structured illumination microscopy data. *Methods Appl. Fluoresc.* **2015**, *3*, 014002.

(31) Zhang, Y.; Lang, S.; Wang, H.; Liao, J.; Gong, Y. Super-resolution algorithm based on Richardson−Lucy deconvolution for three-dimensional structured illumination microscopy. *J. Opt. Soc. Am. A* **2019**, *36*, 173−178.

(32) Sibarita, J.-B. *Microscopy Techniques*; Springer, 2005; pp 201−243.

(33) Akyüz, A. O.; Reinhard, E. Noise reduction in high dynamic range imaging. *J. Vis. Commun. Image Represent.* **2007**, *18*, 366−376.

(34) Xie, Q.; Wang, J.; Jiang, Y.; Liang, J.; Qu, E.; Ren, L. Far-field super-oscillation imaging based on the super-oscillation elements and PSF feature extraction algorithm. *J. Opt. Soc. Am. A* **2018**, *35*, 491−495.